

# Experimental Phase Equilibria Studies in the FeO-Fe<sub>2</sub>O<sub>3</sub>-CaO-Al<sub>2</sub>O<sub>3</sub> System in Air



SIYU CHENG , MAKSYM SHEVCHENKO , PETER C. HAYES ,  
and EVGUENI JAK

The CaO·3(Al,Fe)<sub>2</sub>O<sub>3</sub> (C(A,F)<sub>3</sub>) phase forms a solid solution in the FeO-Fe<sub>2</sub>O<sub>3</sub>-CaO-Al<sub>2</sub>O<sub>3</sub> system and is an end member of the SFCA (Silico-Ferrite of Calcium and Aluminum) suite of solid solutions observed in industrial iron ore sinters. SFCA acts as a bonding phase in these sinter materials so an accurate description of the phase equilibria and thermodynamic properties of this phase can be used to assist in the design and operation of Fe-sintering and Fe-making processes. New experimental data are reported on the liquidus and sub-liquidus phase equilibria in the iron-rich region of the FeO-Fe<sub>2</sub>O<sub>3</sub>-CaO-Al<sub>2</sub>O<sub>3</sub> system in air. The study was undertaken using equilibration/quenching and microanalysis techniques enabling the compositions of the liquid and solid phases in equilibrium at high temperature to be directly and accurately measured. The compositional limits of the C(A,F)<sub>3</sub> phase and associations with the primary phase fields of CA [CaO·(Al,Fe)<sub>2</sub>O<sub>3</sub>], CA<sub>2</sub> [CaO·2(Al,Fe)<sub>2</sub>O<sub>3</sub>], CA<sub>6</sub> [CaO·6(Al,Fe)<sub>2</sub>O<sub>3</sub>], Hematite [(Fe,Al)<sub>2</sub>O<sub>3</sub>], Spinel [(Fe,Ca)O·(Fe,Al)<sub>2</sub>O<sub>3</sub>], C<sub>2</sub>F [2CaO·(Fe,Al)<sub>2</sub>O<sub>3</sub>], C<sub>2</sub>F<sub>3</sub>A (2CaO·3Fe<sub>2</sub>O<sub>3</sub>·Al<sub>2</sub>O<sub>3</sub>), CF [CaO·(Fe,Al)<sub>2</sub>O<sub>3</sub>], and CF<sub>2</sub> [CaO·2(Fe,Al)<sub>2</sub>O<sub>3</sub>] have been determined in the high-iron, low-melting temperature region of the system. The C(A,F)<sub>3</sub> is found to be stable over a wide range of temperatures (1213 °C to 1400 °C) and alumina compositions (3.3 to 33.6 mol pct AlO<sub>1.5</sub>). The solid-phase C<sub>2</sub>F<sub>3</sub>A (2CaO·3Fe<sub>2</sub>O<sub>3</sub>·Al<sub>2</sub>O<sub>3</sub>), which is isostructural to SFCA-I indicated by previous researchers, has been found to be stable up to 1225 °C in the FeO-Fe<sub>2</sub>O<sub>3</sub>-CaO-Al<sub>2</sub>O<sub>3</sub> system in air.

<https://doi.org/10.1007/s11663-021-02198-3>

© The Minerals, Metals & Materials Society and ASM International 2021

## I. INTRODUCTION

THE Silico-Ferrite of Calcium and Aluminum (SFCA, where S, F, C, and A in this paper indicate SiO<sub>2</sub>, “Fe<sub>2</sub>O<sub>3</sub>,” CaO, and Al<sub>2</sub>O<sub>3</sub>, respectively) is a key phase in the iron ore-sintering process as it constitutes a large proportion of materials present in the industrial sinter products (see Figure 1) and is believed to enhance the reducibility and mechanical strength of the sinters.<sup>[1]</sup> This phase extends towards the FeO-Fe<sub>2</sub>O<sub>3</sub>-CaO-SiO<sub>2</sub> sub-system as Silico-Ferrite of Calcium (SFC) and towards the FeO-Fe<sub>2</sub>O<sub>3</sub>-CaO-Al<sub>2</sub>O<sub>3</sub> sub-system as the C(A,F)<sub>3</sub> [CaO·3(Al,Fe)<sub>2</sub>O<sub>3</sub>] solid solution.

Previous experimental studies of phase equilibria relating to the SFCA phase have been principally focused on (i) the FeO-Fe<sub>2</sub>O<sub>3</sub>-CaO-SiO<sub>2</sub> system in air;<sup>[2–4]</sup> (ii) the FeO-Fe<sub>2</sub>O<sub>3</sub>-CaO-SiO<sub>2</sub> system at selected

oxygen partial pressures<sup>[5,6]</sup>; and (iii) liquidus and sub-liquidus regions in the FeO-Fe<sub>2</sub>O<sub>3</sub>-CaO-Al<sub>2</sub>O<sub>3</sub> system<sup>[7–13]</sup>; and (iv) SFCA as well as the hematite liquidus in the FeO-Fe<sub>2</sub>O<sub>3</sub>-CaO-SiO<sub>2</sub>-Al<sub>2</sub>O<sub>3</sub> system in air.<sup>[8,14]</sup> The aim of the present study is to determine the phase equilibria in the FeO-Fe<sub>2</sub>O<sub>3</sub>-CaO-Al<sub>2</sub>O<sub>3</sub> system in air, with a focus on phase relations and thermodynamic limits of the C(A,F)<sub>3</sub> [CaO·3(Al,Fe)<sub>2</sub>O<sub>3</sub>] solid solution.

## II. LITERATURE REVIEW

The currently accepted version of the “Fe<sub>2</sub>O<sub>3</sub>”-CaO-Al<sub>2</sub>O<sub>3</sub> liquidus surface in air in Slag Atlas,<sup>[15]</sup> was constructed based principally on the experimental studies by Dayal and Glasser,<sup>[16]</sup> and Lister and Glasser.<sup>[17]</sup> The system was investigated for temperatures from 1178 °C to 1527 °C using an equilibration and quenching method followed by optical microscopy, X-ray powder diffraction, and wet chemical analysis. The C(A,F)<sub>3</sub> solid solution was reported to be stable on the liquidus surface up to 1435 °C, with its composition lying on the join between “CA<sub>3</sub>” (CaO·3Al<sub>2</sub>O<sub>3</sub>) and “CF<sub>3</sub>” (CaO·3Fe<sub>2</sub>O<sub>3</sub>) between 44.5 and 81.5 mol pct CF<sub>3</sub>. Malysheva *et al.*<sup>[18]</sup> studied this system using a

SIYU CHENG, MAKSYM SHEVCHENKO, PETER C. HAYES and EVGUENI JAK are with the PYROSEARCH, Pyrometallurgy Innovation Centre, School of Chemical Engineering, The University of Queensland, Brisbane, QLD, 4072, Australia. Contact e-mail: s.cheng@uq.edu.au

Manuscript submitted November 4, 2020; accepted April 18, 2021.

Article published online May 17, 2021.

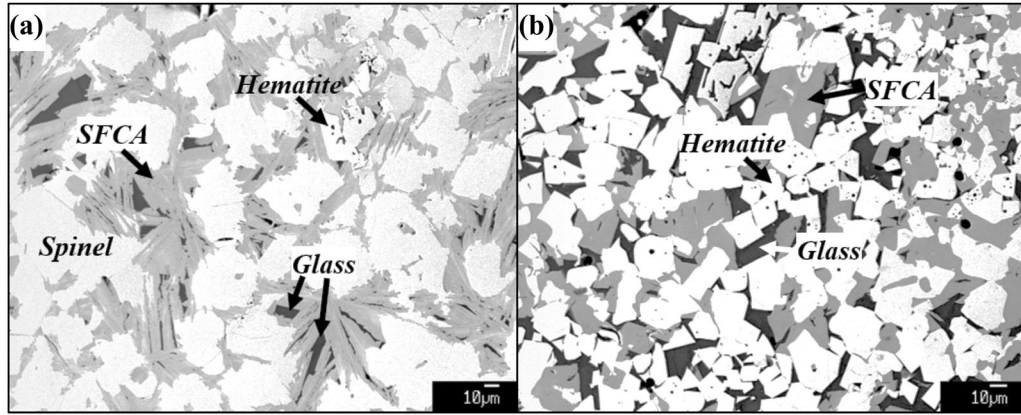


Fig. 1—Backscattered electron images showing typical microstructures of industrial iron ore-sintering products containing (a) platy and (b) blocky SFCA, associated with the hematite, spinel, and amorphous glass phases.

combination of microprobe and wet chemical analyses. They reported variable CaO concentrations in the C(A,F)<sub>3</sub> solid solution, although departing from the “CA<sub>3</sub>” – “CF<sub>3</sub>” join, within the following limits: 12-17 wt pct CaO, 2-30 wt pct Al<sub>2</sub>O<sub>3</sub>, and 58-51 wt pct Fe<sub>2</sub>O<sub>3</sub> from 1130 °C to 1260 °C. Arakcheeva *et al.*<sup>[19,20]</sup> reported a new aluminum-calcium ferrite phase (CaFe<sub>3</sub>AlO<sub>7</sub>, expressed as “C<sub>2</sub>F<sub>3</sub>A (2CaO·3-Fe<sub>2</sub>O<sub>3</sub>·Al<sub>2</sub>O<sub>3</sub>)” in the present study) at 1170 °C in the “Fe<sub>2</sub>O<sub>3</sub>”-CaO-Al<sub>2</sub>O<sub>3</sub> system in air having a composition of Ca<sub>7.12</sub>Fe<sub>0.88</sub><sup>2+</sup>Fe<sub>23.82</sub><sup>3+</sup>Al<sub>8.18</sub>O<sub>56</sub>, this phase is not included in the phase diagram proposed by Dayal and Glasser.<sup>[16]</sup> This new compound, having an overall stoichiometry of M<sub>20</sub>O<sub>28</sub>, was later found to be isostructural to “SFCA-I.”<sup>[21,22]</sup> Mumme *et al.*<sup>[22]</sup> also reported a Si-free SFCA-I in the “Fe<sub>2</sub>O<sub>3</sub>”-CaO-Al<sub>2</sub>O<sub>3</sub> system to be Ca<sub>3.18</sub>Fe<sub>0.82</sub><sup>2+</sup>Fe<sub>14.66</sub><sup>3+</sup>Al<sub>1.34</sub>O<sub>28</sub>, having a lower Al<sub>2</sub>O<sub>3</sub> concentration than the SFCA-I reported by Arakcheeva *et al.*<sup>[19,20]</sup> In a later investigation,<sup>[21]</sup> Mumme reported another Si-free SFCA type (Ca<sub>2</sub>Fe<sub>7</sub>Al<sub>5</sub>O<sub>20</sub>, or CF<sub>1.25</sub>A<sub>1.75</sub>) having an overall stoichiometry of M<sub>14</sub>O<sub>20</sub><sup>[23,24]</sup> formed in the “Fe<sub>2</sub>O<sub>3</sub>”-CaO-Al<sub>2</sub>O<sub>3</sub> system. In the same study,<sup>[21]</sup> SFCA-II with a stoichiometry of M<sub>34</sub>O<sub>48</sub> (Ca<sub>5.1</sub>Al<sub>9.3</sub>Fe<sub>18.7</sub><sup>3+</sup>Fe<sub>0.9</sub>O<sub>48</sub>) was also reported, although it has not been found in industrial sinters.<sup>[25]</sup> To date, different crystal structures of SFCA (SFCA, SFCA-I, and SFCA-II) have been reported,<sup>[19–24]</sup> although the phase relations between them in the FeO-Fe<sub>2</sub>O<sub>3</sub>-CaO-SiO<sub>2</sub>-Al<sub>2</sub>O<sub>3</sub> system in air are yet to be fully characterized. The compositions of the different types of SFCA in the “Fe<sub>2</sub>O<sub>3</sub>”-CaO-SiO<sub>2</sub>-Al<sub>2</sub>O<sub>3</sub> system are summarized and schematically shown in Figure 2.

### III. EXPERIMENTAL METHODOLOGY

The high-temperature equilibration/quenching/EPMA measurement approach used in the present study, developed by the authors,<sup>[26,27]</sup> has been described in detail in previous publications.<sup>[4,28–30]</sup> A 4-point test approach<sup>[27]</sup> was applied to confirm the achievement of equilibrium in each case, which includes (i) test of the effect of equilibration time; (ii) analysis of

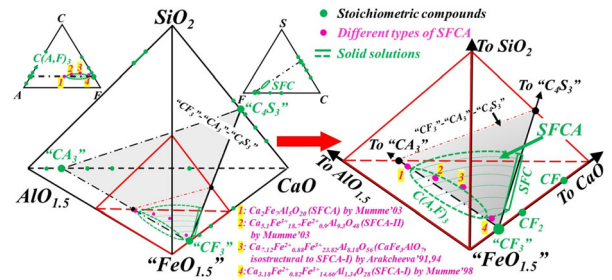


Fig. 2—Schematic diagrams showing the compositions reported of the different types of Si-free SFCA solid solutions in the FeO-Fe<sub>2</sub>O<sub>3</sub>-CaO-Al<sub>2</sub>O<sub>3</sub> system in air.

the homogeneity of the phases; (iii) evaluation of the effect of starting composition and phase assemblage on the approach toward the equilibrium point; and (iv) systematic analysis of reactions specific to the system.

The initial bulk mixtures used in the present study were prepared by mixing, i) high-purity powders of Fe<sub>2</sub>O<sub>3</sub> (99.9 wt pct), Al<sub>2</sub>O<sub>3</sub> (99.9 wt pct) supplied by Sigma-Aldrich Co, NSW, Australia, and ii) a pre-melted CaO-Fe<sub>2</sub>O<sub>3</sub> master slag at 48 mol pct CaO. Each of the samples for the equilibration runs (< 0.3 g) was taken from the bulk mixture and pressed into a pellet using a tool steel die. The initial compositions of the mixtures were selected so that, at the equilibration temperature, one or more crystalline phases would be present in equilibrium with liquid slag. The sample bulk composition was selected targeting the volume fraction of solids to be below 50 pct, and preferably approximately 10 pct at the equilibration temperature. This enables rapid equilibration to be achieved and the liquid to be retained as an amorphous or glass phase on quenching by (i) reducing the availability of nuclei and surfaces for crystallization and (ii) reducing the “enthalpy” introduced by solids needed to be conducted into the quenching media.

The platinum substrates used for supporting the samples during equilibration were prepared by winding pure platinum wire (99.99 wt pct Pt, 0.5 mm diameter, supplied by Johnson Matthey Ltd, Tullamarine VIC,

Australia) into a spiral shape. The design of this substrate maximizes the area of direct contact between the molten sample and the quenching medium, which enables rapid quenching of the sample.<sup>[3,4]</sup>

All equilibration experiments were carried out in a vertical reaction tube (impervious recrystallized alumina, 30-mm inner diameter) within an electrical resistance lanthanum chromite-heated furnace. The samples were placed in the uniform hot zone of the furnace immediately adjacent to a working thermocouple that was inserted into a recrystallized alumina sheath to monitor the actual sample temperature. The working thermocouple (Pt-Pt-13 pct Rh) was calibrated against a standard thermocouple (supplied by the National Measurement Institute of Australia, NSW, Australia). The overall absolute temperature accuracy of each experiment was estimated to be  $\pm 3$  K. The bottom of the reaction tube remained open throughout the experiments to ensure ambient air atmosphere inside,  $p(\text{O}_2) = 0.21$  atm.

The samples were suspended in the hot zone of the furnace by Kanthal support wire (Fe-Cr-Al alloy, 0.7 mm diameter). For temperatures higher than 1450 °C, a 0.5-mm-diameter pure Pt wire was used to extend the support so that the Kanthal wire is not in the hot zone. The samples were pre-melted for 15 to 30 minutes at temperatures 5 °C to 100 °C above the equilibration temperature, to facilitate the formation of a homogeneous liquid slag in each case. Some samples were then pre-crystallized for another 15 to 30 minutes at temperatures 5 °C to 20 °C below the equilibration temperature, followed by equilibration at the final target temperature for the required time. The pre-melt and pre-crystallization procedures are designed to confirm the achievement of equilibrium from different thermal trajectories. At the end of the equilibration process, the samples were released and rapidly quenched into  $\text{CaCl}_2$ -containing brine ( $< 253$  K ( $- 20$  °C)). The samples were then washed thoroughly in water and ethanol before being dried on a hot plate and mounted in epoxy resin. Polished cross sections were prepared using conventional metallographic techniques.

The samples were first examined by optical microscopy and then carbon coated, and the phase compositions were measured using an electron probe X-ray microanalysis technique with wavelength dispersive detectors (JEOL 8200L EPMA, Japan Electron Optics Ltd., Tokyo, Japan). In the present study, the EPMA is operated at 15 kV accelerating voltage and 20 nA probe current using the standard Duncumb–Philibert atomic number, absorption, and fluorescence (ZAF) correction supplied by JEOL.<sup>[31–33]</sup> The standards used (supplied by Charles M. Taylor Co., Stanford, CA) include wollastonite ( $\text{CaSiO}_3$ ) for calcium ( $K\alpha$ ) calibration, hematite ( $\text{Fe}_2\text{O}_3$ ) for iron ( $K\alpha$ ) calibration, corundum ( $\text{Al}_2\text{O}_3$ ) for alumina ( $K\alpha$ ) calibration, and in some cases, platinum ( $M\alpha$ ) to test for possible contamination. Fe is always present in the slag in two oxidation states:  $\text{Fe}^{2+}$  and  $\text{Fe}^{3+}$ . Only the concentrations of the metal cations were measured by EPMA in the present study. All cation concentrations measured with EPMA were then recalculated to selected oxidation states (*i.e.*,  $\text{FeO}_{1.5}$ ,

$\text{CaO}$ , and  $\text{AlO}_{1.5}$ ) and normalized to 100 pct for presentation purposes only. The normalized phase compositions and original sums of elements or oxides from EPMA analyses are provided in tabular form. The total compositions before normalization to 100 pct are also reported in Table I, indicated as the “original total.”

The ability to quench the liquid slag phase to ambient temperature without the onset of crystallization was found to depend on the composition of the slag and the equilibration temperature. The most significant problems were observed with low- $\text{Al}_2\text{O}_3$  slags at high temperatures, at or above 1300 °C, where the glassy homogeneous areas, believed to be formed at the surfaces directly contacting the quenching medium, were only a small proportion of the quenched melt. For these samples, the approach taken to obtain accurate, repeatable, and objective measurements of the average compositions of the liquid slag phase by the use of EPMA was similar to that described by Nikolic *et al.*<sup>[34]</sup>: an average of at least 20 points in the best quenched area (usually, near the surface) was used, with a standard deviation of composition not exceeding 1 mol pct. In cases where melt crystallization was rapid, the experiments were repeated until an area of sufficiently well-quenched microstructure was found. Increasing the probe diameter to 5 to 50  $\mu\text{m}$  resulted in reduced variability of the measured liquid slag compositions.<sup>[35]</sup>

The standard ZAF correction supplied by JEOL was further improved following the same approach as described in detail in previous publications.<sup>[4,28]</sup> Using stoichiometric  $\text{Ca}_2\text{Fe}_2\text{O}_5$ ,  $\text{CaFe}_2\text{O}_4$  and  $\text{CaFe}_4\text{O}_7$  as secondary standards, an analytical expression is developed to correct all cation concentrations in the “ $\text{FeO}_{1.5}$ ”- $\text{CaO}$ - $\text{Al}_2\text{O}_3$  system:

$$x(\text{CaO})^{\text{corr}} = x(\text{CaO}) - x(\text{CaO})x(\text{FeO}_{1.5}) \\ (0.0208 + 0.0119(x(\text{FeO}_{1.5}) - x(\text{CaO}))),$$

$$x(\text{AlO}_{1.5})^{\text{corr}} = x(\text{AlO}_{1.5}),$$

$$x(\text{FeO}_{1.5})^{\text{corr}} = 1 - x(\text{CaO})^{\text{corr}} - x(\text{AlO}_{1.5})^{\text{corr}},$$

where  $x(\text{CaO}$ ,  $\text{FeO}_{1.5}$ ,  $\text{AlO}_{1.5})$  are the cation molar fractions following JEOL ZAF correction, and  $x(\text{CaO}$ ,  $\text{FeO}_{1.5}$ ,  $\text{AlO}_{1.5})^{\text{corr}}$  are the final corrected cation molar fractions. This approach is similar to that employed in the previous studies by the authors.<sup>[29,36]</sup> The accuracy of the compositions measured was estimated to be within 1 wt pct.

## IV. RESULTS

### A. Phase Equilibria and Microstructures

Backscattered electron micrographs of typical microstructures obtained on equilibration in the iron-rich region in the  $\text{FeO}$ - $\text{FeO}_{1.5}$ - $\text{CaO}$ - $\text{AlO}_{1.5}$  system in air, are shown in Figures 3(a) through (f). From the results of electron probe microanalysis, the following phases

**Table I. Molar Compositions of Initial Bulk Mixtures Selected in Each Equilibration Run, and Molar Compositions and Standard Deviations of the Compositions of the Phases After Equilibration in the “FeO<sub>1.5</sub>”-CaO-AlO<sub>1.5</sub> System in Air, Measured by EPMA**

No.	Initial Mixture Compositions (Mol Pct)			Temp.°C	Phases	Phase Compositions (Mol Pct)						Original Total (Wt Pct)
	AlO <sub>1.5</sub>	FeO <sub>1.5</sub>	CaO			AlO <sub>1.5</sub>	Stdev.	FeO <sub>1.5</sub>	Stdev.	CaO	Stdev.	
Hematite [(Fe,Al) <sub>2</sub> O <sub>3</sub> ] primary phase field												
1	8.7	75.6	15.7	1350	liquid	9.5	0.07	71.4	0.32	19.0	0.32	98.8
					hematite	6.5	0.10	93.5	0.10	0.0	0.00	100.2
Spinel [(Fe,Ca)O·(Fe,Al) <sub>2</sub> O <sub>3</sub> ] primary phase field												
2	10.3	79.1	10.5	1400	liquid	11.8	0.09	68.9	0.79	19.3	0.80	100.5
					spinel	9.3	0.06	88.2	0.07	2.5	0.04	102.0
3	4.7	82.7	12.6	1370	liquid	5.3	0.07	75.9	0.96	18.8	0.94	100.1
					spinel	4.1	0.03	92.6	0.06	3.3	0.05	101.6
CA <sub>6</sub> [CaO·6(Al,Fe) <sub>2</sub> O <sub>3</sub> ] primary phase field												
4	27.7	60.2	12.2	1500	liquid	26.2	0.47	60.7	1.00	13.1	0.96	101.1
					CA <sub>6</sub>	71.1	0.48	21.2	0.50	7.6	0.04	101.0
5	26.6	55.1	18.3	1400	liquid	23.1	0.15	57.4	0.37	19.5	0.47	100.7
					CA <sub>6</sub>	59.9	0.78	32.4	0.79	7.7	0.08	101.5
C(A,F) <sub>3</sub> [CaO·3(Al,Fe) <sub>2</sub> O <sub>3</sub> ] primary phase field												
6	26.6	55.1	18.3	1380	liquid	22.3	0.17	56.1	0.81	21.6	0.84	100.3
					C(A,F) <sub>3</sub>	33.6	0.25	52.8	0.26	13.6	0.14	101.2
7	20.1	66.2	13.7	1360	liquid	11.3	0.34	67.7	0.91	21.0	0.93	99.9
					C(A,F) <sub>3</sub>	22.1	0.33	65.2	0.28	12.8	0.14	100.7
8	21.7	59.9	18.4	1350	liquid	17.3	0.08	61.4	0.14	21.3	0.12	100.3
					C(A,F) <sub>3</sub>	29.8	0.24	56.6	0.21	13.7	0.11	101.0
9	14.2	67.8	18.0	1350	liquid	11.3	0.09	68.6	0.67	20.1	0.72	100.3
					C(A,F) <sub>3</sub>	21.3	0.19	65.7	0.17	13.1	0.07	101.2
10	20.0	53.2	26.8	1300	liquid	19.7	0.09	52.6	0.21	27.7	0.20	100.3
					C(A,F) <sub>3</sub>	28.7	0.19	55.7	0.22	15.6	0.06	101.1
11	18.2	58.0	23.9	1300	liquid	14.5	0.11	57.5	0.23	27.9	0.29	100.0
					C(A,F) <sub>3</sub>	25.4	0.16	59.1	0.19	15.5	0.10	100.5
12	14.2	67.8	18.0	1300	liquid	9.0	0.07	66.7	0.10	24.3	0.08	99.9
					C(A,F) <sub>3</sub>	16.8	0.34	68.0	0.25	15.2	0.16	101.0
13	6.9	70.6	22.5	1300	liquid	6.4	0.07	70.8	0.16	22.8	0.14	100.1
					C(A,F) <sub>3</sub>	13.2	0.18	72.2	0.22	14.7	0.10	100.5
14	20.0	53.2	26.8	1250	liquid	18.0	0.06	51.6	0.11	30.5	0.09	100.2
					C(A,F) <sub>3</sub>	27.5	0.37	56.2	0.39	16.3	0.17	100.9
15	18.2	58.0	23.9	1250	liquid	13.4	0.09	56.8	0.35	29.8	0.35	100.2
					C(A,F) <sub>3</sub>	24.7	0.39	59.4	0.31	15.8	0.15	100.4
16	10.0	63.7	26.3	1250	liquid	8.7	0.04	62.4	0.10	28.8	0.09	99.5
					C(A,F) <sub>3</sub>	15.3	0.22	67.3	0.14	17.4	0.21	100.2
17	14.2	67.8	18.0	1250	liquid	8.4	0.11	62.6	0.22	29.0	0.28	100.2
					C(A,F) <sub>3</sub>	14.7	0.17	67.8	0.22	17.4	0.12	100.6
18	6.9	70.6	22.5	1250	liquid	4.6	0.07	69.1	0.14	26.3	0.14	99.5
					C(A,F) <sub>3</sub>	10.1	0.70	73.5	0.52	16.4	0.25	100.5
19	20.0	53.2	26.8	1225	liquid	16.5	0.18	51.2	0.16	32.3	0.30	100.1
					C(A,F) <sub>3</sub>	27.6	0.14	56.1	0.24	16.4	0.17	100.8
20	10.0	63.7	26.3	1210	liquid	7.7	0.09	60.5	0.13	31.7	0.19	99.8
					C(A,F) <sub>3</sub>	13.9	0.73	67.8	0.66	18.3	0.16	100.4
CA <sub>2</sub> [CaO·2(Al,Fe) <sub>2</sub> O <sub>3</sub> ] primary phase field												
21	28.4	49.9	21.7	1400	liquid	27.7	0.27	50.5	0.13	21.8	0.21	100.8
					CA <sub>2</sub>	72.1	0.30	8.0	0.27	19.9	0.08	101.3
C <sub>2</sub> F [2CaO·(Fe,Al) <sub>2</sub> O <sub>3</sub> ] primary phase field												
22	10.5	50.3	39.2	1300	liquid	11.0	0.06	53.5	0.17	35.5	0.18	100.0
					C <sub>2</sub> F	8.3	0.06	41.9	0.16	49.8	0.15	100.4
23	10.5	50.3	39.2	1250	liquid	11.3	0.09	55.3	0.12	33.4	0.15	98.9
					C <sub>2</sub> F	8.2	0.18	41.8	0.25	50.0	0.15	100.2
Spinel [(Fe,Ca)O·(Fe,Al) <sub>2</sub> O <sub>3</sub> ] - CA <sub>6</sub> [CaO·6(Al,Fe) <sub>2</sub> O <sub>3</sub> ] univariant line												
24	27.7	60.2	12.2	1450	liquid	21.8	0.16	62.8	0.72	15.4	0.79	100.8
					spinel	18.7	0.12	79.9	0.12	1.4	0.04	102.4
					CA <sub>6</sub>	62.6	0.19	29.6	0.18	7.8	0.03	101.3
25	21.0	71.8	7.2	1440	liquid	21.2	0.51	60.3	0.97	18.5	0.70	99.7
					spinel	17.7	0.17	80.8	0.18	1.5	0.03	102.0
					CA <sub>6</sub>	61.1	0.37	31.4	0.37	7.6	0.02	99.6

Table I. continued

No.	Initial Mixture Compositions (Mol Pct)			Temp. °C	Phases	Phase Compositions (Mol Pct)						Original Total (Wt Pct)
	AlO <sub>1.5</sub>	FeO <sub>1.5</sub>	CaO			AlO <sub>1.5</sub>	Stdev.	FeO <sub>1.5</sub>	Stdev.	CaO	Stdev.	
CA <sub>6</sub> [CaO·6(Al,Fe) <sub>2</sub> O <sub>3</sub> ] - C(A,F) <sub>3</sub> [CaO·3(Al,Fe) <sub>2</sub> O <sub>3</sub> ] univariant line												
26	21.7	59.9	18.4	1400	liquid	21.2	0.15	60.2	0.40	18.6	0.50	100.5
					CA <sub>6</sub>	55.6	0.26	36.8	0.35	7.6	0.09	100.8
					C(A,F) <sub>3</sub>	31.4	0.12	56.6	0.15	12.0	0.03	100.6
Spinel [(Fe,Ca)O·(Fe,Al) <sub>2</sub> O <sub>3</sub> ] - C(A,F) <sub>3</sub> [CaO·3(Al,Fe) <sub>2</sub> O <sub>3</sub> ] univariant line												
27	20.1	66.2	13.7	1400	liquid	17.0	0.30	64.1	0.82	19.0	0.64	99.2
					spinel	13.4	0.19	84.5	0.16	2.1	0.05	101.5
					C(A,F) <sub>3</sub>	25.3	0.22	64.8	0.28	9.9	0.11	100.5
28	20.1	66.2	13.7	1380	liquid	13.0	0.13	67.8	0.40	19.2	0.43	100.1
					spinel	10.1	0.14	87.1	0.09	2.8	0.15	101.4
					C(A,F) <sub>3</sub>	24.6	0.23	63.0	0.21	12.4	0.06	100.8
Hematite [(Fe,Al) <sub>2</sub> O <sub>3</sub> ] - C(A,F) <sub>3</sub> [CaO·3(Al,Fe) <sub>2</sub> O <sub>3</sub> ] univariant line												
29	6.9	75.4	17.7	1300	liquid	5.6	0.08	71.7	0.20	22.8	0.19	100.0
					hematite	3.4	0.09	96.6	0.09	0.0	0.00	100.2
					C(A,F) <sub>3</sub>	12.3	0.22	73.1	0.23	14.7	0.10	100.3
30	5.8	73.6	20.6	1275	liquid	4.0	0.07	71.8	0.16	24.2	0.15	100.0
					hematite	2.3	0.02	97.7	0.02	0.0	0.02	99.2
					C(A,F) <sub>3</sub>	8.8	0.53	75.4	0.46	15.8	0.11	99.6
31	5.8	73.6	20.6	1250	liquid	3.3	0.37	69.8	0.92	26.9	0.72	100.2
					hematite	1.6	0.40	98.1	0.50	0.3	0.10	99.0
					C(A,F) <sub>3</sub>	7.5	0.78	75.7	0.70	16.8	0.24	100.3
C(A,F) <sub>3</sub> [CaO·3(Al,Fe) <sub>2</sub> O <sub>3</sub> ] - CF <sub>2</sub> [CaO·2(Fe,Al) <sub>2</sub> O <sub>3</sub> ] univariant line												
32	2.0	73.7	24.2	1220	liquid	1.8	0.05	69.5	0.18	28.7	0.15	99.9
					C(A,F) <sub>3</sub>	3.5	0.18	78.5	0.15	18.0	0.09	100.1
					CF <sub>2</sub>	1.5	0.04	78.3	0.12	20.2	0.09	99.9
33	2.0	73.7	24.2	1213	liquid	1.8	0.09	69.4	0.27	28.7	0.29	97.7
					C(A,F) <sub>3</sub>	3.3	0.25	79.0	0.39	17.6	0.25	98.4
					CF <sub>2</sub>	1.5	0.07	78.6	0.19	20.0	0.16	98.1
C(A,F) <sub>3</sub> [CaO·3(Al,Fe) <sub>2</sub> O <sub>3</sub> ] - CA <sub>2</sub> [CaO·2(Al,Fe) <sub>2</sub> O <sub>3</sub> ] univariant line												
34	28.4	49.9	21.7	1350	liquid	23.7	0.12	51.9	0.17	24.4	0.14	99.8
					C(A,F) <sub>3</sub>	33.0	0.37	52.5	0.33	14.5	0.07	101.1
					CA <sub>2</sub>	71.1	0.71	9.0	0.72	19.9	0.11	101.2
35	34.3	39.4	26.2	1300	liquid	22.9	0.10	48.8	0.14	28.3	0.10	100.4
					C(A,F) <sub>3</sub>	30.7	0.08	53.6	0.08	15.7	0.10	100.1
					CA <sub>2</sub>	70.7	0.41	9.3	0.43	20.0	0.05	100.2
C(A,F) <sub>3</sub> [CaO·3(Al,Fe) <sub>2</sub> O <sub>3</sub> ] - CA [CaO·(Al,Fe) <sub>2</sub> O <sub>3</sub> ] univariant line												
36	25.5	46.9	27.6	1250	liquid	21.0	0.11	48.1	0.15	30.9	0.10	99.8
					C(A,F) <sub>3</sub>	28.8	0.2	54.6	0.18	16.7	0.11	100.0
					CA	58.5	0.31	8.2	0.32	33.3	0.11	99.0
C(A,F) <sub>3</sub> [CaO·3(Al,Fe) <sub>2</sub> O <sub>3</sub> ] - C <sub>2</sub> F <sub>3</sub> A [2CaO·3Fe <sub>2</sub> O <sub>3</sub> ·Al <sub>2</sub> O <sub>3</sub> ] univariant line												
37	20.0	53.2	26.8	1225	liquid	14.4	0.05	53.8	0.22	31.8	0.25	99.7
					C(A,F) <sub>3</sub>	27.6	0.12	56.1	0.22	16.4	0.15	100.8
					C <sub>2</sub> F <sub>3</sub> A	20.8	0.16	60.9	0.02	18.2	0.13	100.1
38	16.7	53.5	29.8	1220	liquid	15.6	0.10	51.8	0.14	32.7	0.15	99.2
					C(A,F) <sub>3</sub>	24.2	0.33	59.0	0.28	16.9	0.09	99.0
					C <sub>2</sub> F <sub>3</sub> A	21.7	0.60	59.9	0.52	18.4	0.15	98.3
39	16.7	53.5	29.8	1215	liquid	15.7	0.08	51.8	0.22	32.5	0.22	99.6
					C(A,F) <sub>3</sub>	24.2	0.38	58.6	0.34	17.2	0.17	99.8
					C <sub>2</sub> F <sub>3</sub> A	21.2	0.27	60.2	0.27	18.6	0.20	99.9
CF <sub>2</sub> [CaO·2(Fe,Al) <sub>2</sub> O <sub>3</sub> ] - CF [CaO·(Fe,Al) <sub>2</sub> O <sub>3</sub> ] univariant line												
40	2.0	73.7	24.2	1210	liquid	1.9	0.18	68.9	0.67	29.2	0.75	98.2
					CF <sub>2</sub>	1.6	0.06	78.3	0.14	20.1	0.08	98.4
					CF	0.6	0.12	66.4	0.29	33.0	0.20	97.9
CA <sub>6</sub> [CaO·6(Al,Fe) <sub>2</sub> O <sub>3</sub> ] - CA <sub>2</sub> [CaO·2(Al,Fe) <sub>2</sub> O <sub>3</sub> ] univariant line												
41	47.1	36.1	16.8	1450	liquid	31.9	0.25	47.1	0.42	21.0	0.59	100.3
					CA <sub>6</sub>	72.7	0.26	19.6	0.27	7.7	0.15	101.0
					CA <sub>2</sub>	72.9	0.16	7.2	0.16	19.9	0.09	99.4

Table I. continued

No.	Initial Mixture Compositions (Mol Pct)			Temp. °C	Phases	Phase Compositions (Mol Pct)						Original Total (Wt Pct)
	AlO <sub>1.5</sub>	FeO <sub>1.5</sub>	CaO			AlO <sub>1.5</sub>	Stdev.	FeO <sub>1.5</sub>	Stdev.	CaO	Stdev.	
CA [CaO·(Al,Fe) <sub>2</sub> O <sub>3</sub> ] - C <sub>2</sub> F [2CaO·(Fe,Al) <sub>2</sub> O <sub>3</sub> ] univariant line												
42	33.6	32.2	34.2	1250	liquid	21.0	0.27	44.6	0.34	34.4	0.26	99.1
					CA	57.9	0.21	8.6	0.23	33.5	0.10	99.9
					C <sub>2</sub> F	12.7	0.21	37.3	0.10	50.0	0.13	100.4
43	20.1	41.0	38.9	1225	liquid	19.0	0.05	48.0	0.08	33.0	0.08	99.5
					CA	56.7	0.59	9.9	0.61	33.4	0.23	99.9
					C <sub>2</sub> F	12.1	0.17	37.9	0.18	50.0	0.08	100.1
Sub-solidus												
44	20.1	41.0	38.9	1200	C <sub>2</sub> F <sub>3</sub> A	20.0	0.50	61.1	0.54	18.9	0.10	100.4
					CA	56.3	0.12	10.4	0.18	33.3	0.12	100.5
					C <sub>2</sub> F	12.3	0.61	37.8	0.68	49.9	0.12	100.4
45	20.1	41.0	38.9	1150	C <sub>2</sub> F <sub>3</sub> A	18.6	0.72	62.5	0.75	18.9	0.18	100.5
					CA	56.1	0.41	10.7	0.44	33.2	0.05	100.7
					C <sub>2</sub> F	13.3	0.33	36.7	0.38	50.0	0.12	100.5

have been identified to be present in the range of compositions and temperatures investigated: liquid (Liq), hematite [(Fe,Al)<sub>2</sub>O<sub>3</sub>], spinel [(Fe,Ca)O·(Fe,Al)O<sub>2</sub>O<sub>3</sub>], CA [CaO·(Al,Fe)<sub>2</sub>O<sub>3</sub>], CA<sub>2</sub> [CaO·2(Al,Fe)<sub>2</sub>O<sub>3</sub>], CA<sub>6</sub> [CaO·6(Al,Fe)<sub>2</sub>O<sub>3</sub>], C<sub>2</sub>F [2CaO·(Fe,Al)<sub>2</sub>O<sub>3</sub>], CF [CaO·(Fe,Al)<sub>2</sub>O<sub>3</sub>] and CF<sub>2</sub> [CaO·2(Fe,Al)<sub>2</sub>O<sub>3</sub>], C(A,F)<sub>3</sub> [CaO·3(Al,Fe)<sub>2</sub>O<sub>3</sub>], and C<sub>2</sub>F<sub>3</sub>A (2CaO·3Fe<sub>2</sub>O<sub>3</sub>·Al<sub>2</sub>O<sub>3</sub>).

Figure 3(a) shows the microstructure of a sub-solidus sample containing three solids: C<sub>2</sub>F<sub>3</sub>A, C<sub>2</sub>F, and CA. Figures 3(b) through (e) show microstructures containing of the C(A,F)<sub>3</sub> phase in equilibrium with a liquid phase, and the C<sub>2</sub>F<sub>3</sub>A, CA, CA<sub>2</sub>, and spinel phases, respectively. Figure 3(f) shows the liquid in equilibrium with CA<sub>6</sub> and CA<sub>2</sub>.

The liquid phase is retained as a glass on rapid quenching of the samples from the equilibration temperature. The presence of fine microcrystalline in, or instead of, the glassy liquid phase is the result of crystallization that has taken place in the high fluidity slag during the cooling of the samples; these phases and associated structures are artifacts and are not included in the description of the equilibria.

### B. Phase Compositions

The initial bulk mixture compositions, and the measured average molar compositions and standard deviations of the measurements of each phase, are given in Table I. It should be noted that the Fe species in the slag are present in two oxidation states: Fe<sup>2+</sup> and Fe<sup>3+</sup>. The proportions of Fe<sup>3+</sup> in the slags increase with increasing oxygen partial pressures and decreasing temperatures.<sup>[37]</sup> Previous measurements by Dayal and Glasser<sup>[16]</sup> have shown that the concentration of ferrous ions in the liquid slags in air are low, typically less than 2 wt pct FeO even for temperatures up to 1450 °C. Thermodynamic predictions using the FactSage public database<sup>[38–40]</sup> also indicate that the Fe<sup>2+</sup> concentrations in the slags are low in this system within the range of conditions investigated in the present study. Therefore,

all Fe concentrations are recalculated to Fe<sup>3+</sup> for presentation purposes to unambiguously report the compositions of the phases.

The estimated liquid compositions and temperatures of the invariant points in the pseudo-ternary “FeO<sub>1.5</sub>”-CaO-AlO<sub>1.5</sub> system in air are summarized in Table II. The invariant points in the regions where no experimental data have been obtained in the present study are predicted using the FactSage package<sup>[40]</sup> with a separate internal database. The binary invariant temperatures and compositions are taken from Eriksson and Pelton (CaO-AlO<sub>1.5</sub>),<sup>[41]</sup> Probstakova *et al.* (“FeO<sub>1.5</sub>”-AlO<sub>1.5</sub>),<sup>[42]</sup> and Hidayat *et al.* (“FeO<sub>1.5</sub>”-CaO)<sup>[43]</sup> with minor modifications from recent experimental studies by the authors.<sup>[44]</sup> The use of the database, which incorporates all the thermodynamic and phase equilibria data available on the system, ensures that any extrapolations or interpolations undertaken to predict the positions of the phase boundaries obey thermodynamic principles.

### C. Liquidus Surface

Based on the experimental data points obtained in the present study given in Table I, the invariant points from Table II, and the thermodynamic database, the liquidus surface of the “FeO<sub>1.5</sub>”-CaO-AlO<sub>1.5</sub> pseudo-ternary system in air has been constructed. Figure 4 shows the liquidus across the whole of the pseudo-ternary. The system contains the following primary phase fields: lime, corundum, hematite, spinel, CA<sub>6</sub>, C(A,F)<sub>3</sub>, CA<sub>2</sub>, CA, C<sub>2</sub>F<sub>3</sub>A, C<sub>3</sub>A, CF<sub>2</sub>, CF, and C<sub>2</sub>F. The presence of the primary phase field for the ternary compound 2CaO·3Fe<sub>2</sub>O<sub>3</sub>·Al<sub>2</sub>O<sub>3</sub> (C<sub>2</sub>F<sub>3</sub>A) has not previously been reported in the literature.

The experimental liquidus data obtained in the present study have been obtained primarily at liquidus temperatures between 1200 °C and 1450 °C, in the compositional region of the C(A,F)<sub>3</sub> primary phase field, and the boundaries and isotherms in these cases are marked in solid lines. The phase boundaries and the

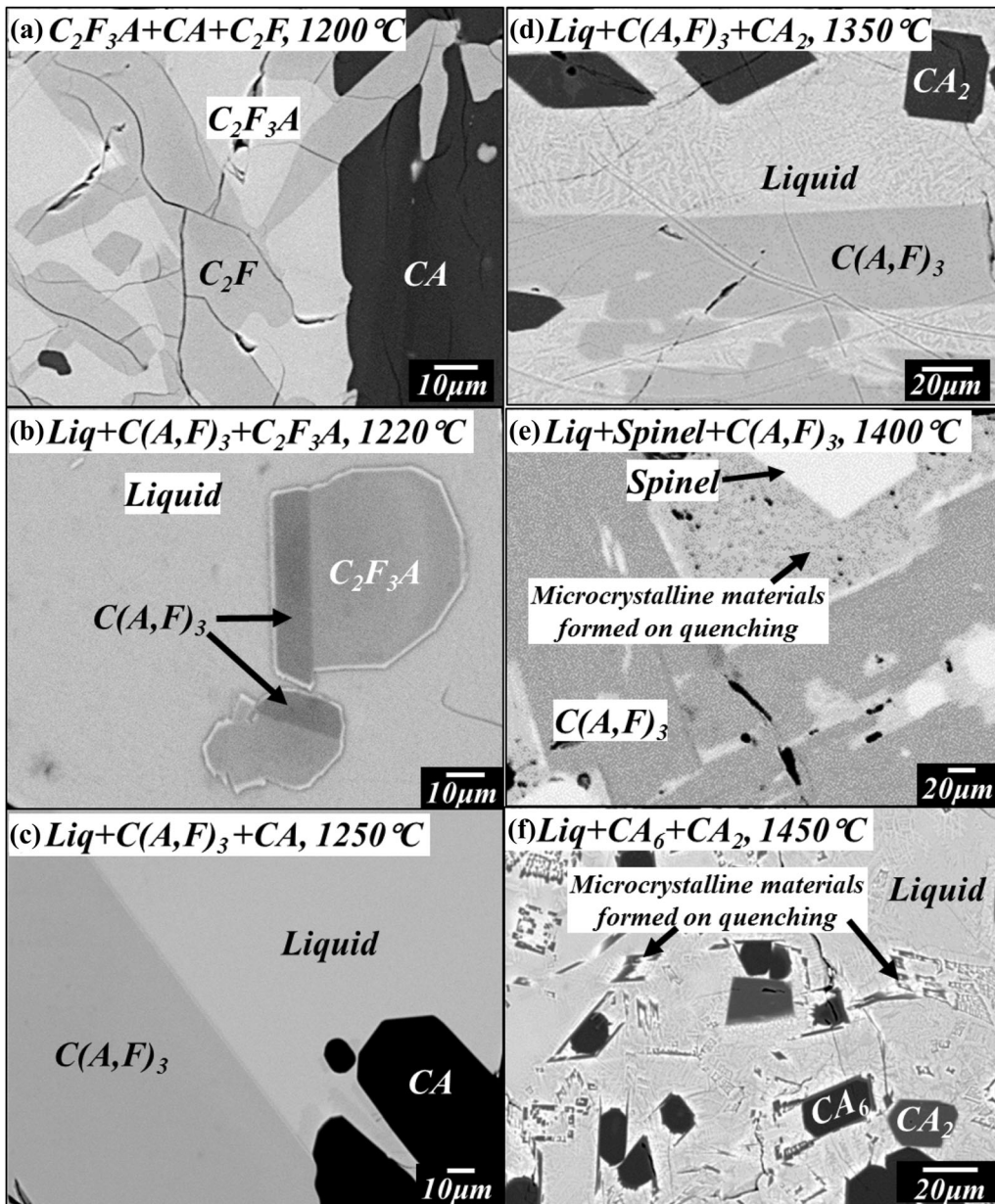


Fig. 3—Backscattered electron images showing typical microstructures of samples in the pseudo-ternary “FeO<sub>1.5</sub>”-CaO-AlO<sub>1.5</sub> in air and the corresponding experiment numbers. (a) C<sub>2</sub>F<sub>3</sub>A + CA + C<sub>2</sub>F, exp. 44; (b) liquid + C(A,F)<sub>3</sub> + C<sub>2</sub>F<sub>3</sub>A, exp. 38; (c) liquid + C(A,F)<sub>3</sub> + CA, exp. 36; (d) liquid + C(A,F)<sub>3</sub> + CA<sub>2</sub>, exp. 34; (e) liquid + spinel + C(A,F)<sub>3</sub>, exp. 27; and (f) liquid + CA<sub>6</sub> + CA<sub>2</sub>, exp. 41.

liquidus isotherms on the diagram at temperatures above 1450 °C are estimated using the thermodynamic database and are marked in both cases with dashed lines. The estimated temperatures (°C) of the invariant and saddle points (a-z) identified in Table II are also marked on the diagram.

Figure 4 shows that the liquidus of the system is dominated by the presence of the primary phase fields of compounds having fixed Ca/(A + F) ratios, these features reflect the extensive solid solutions present in these compounds that have been verified in previous<sup>[7,9-12,18]</sup> and the present experimental studies.

The diagram differs from that previously presented in Slag Atlas<sup>[15]</sup> in two principal respects:

- (a) the C<sub>12</sub>A<sub>7</sub> phase has been previously shown to be a hydrate Ca<sub>12</sub>Al<sub>14</sub>O<sub>32</sub>(OH)<sub>2</sub> and not present in the binary CaO-AlO<sub>1.5</sub> system.<sup>[45,46]</sup> Based on that consideration, the CaO-AlO<sub>1.5</sub> binary<sup>[41]</sup> and the phase boundaries in this region in the “ternary” system in the present study have been amended to reflect the presence of the eutectic between CA-C<sub>2</sub>F-C<sub>3</sub>A at 43.3 mol pct FeO<sub>1.5</sub>, 8.0 mol pct FeO<sub>1.5</sub>, 48.8 mol pct CaO, and 1324 °C (point l on the diagram in Figure 4.
- (b) the primary phase field for C<sub>2</sub>F<sub>3</sub>A has been included, and the phase relations in the low-temperature region centered around the C(A,F)<sub>3</sub> primary

**Table II. Estimated Temperatures and Liquid Compositions of Invariant and Saddle Points for the “FeO<sub>1.5</sub>”-CaO-AlO<sub>1.5</sub> System in Air Based on the Data in Table I, and Estimated Using an Internal Thermodynamic Database**

ID	Estimated (°C)	Type	Phases in Equilibrium with Liquid	Liquid Composition			Liquid Composition			References
				(Mol Pct)			(Wt Pct)			
				AlO <sub>1.5</sub>	“FeO <sub>1.5</sub> ”	CaO	Al <sub>2</sub> O <sub>3</sub>	“Fe <sub>2</sub> O <sub>3</sub> ”	CaO	
CaO-AlO <sub>1.5</sub> system										
(a)	1854	P	Corundum-CA <sub>6</sub>	87.6	0.0	12.4	86.5	0.0	13.5	[41]
(b)	1766	E	CA <sub>6</sub> -CA <sub>2</sub>	82.5	0.0	17.5	81.1	0.0	18.9	
(c)	1599	E	CA <sub>2</sub> -CA	67.9	0.0	32.1	65.8	0.0	34.2	
(d)	1368	E	CA-C <sub>3</sub> A	52.5	0.0	47.5	50.1	0.0	49.9	
(e)	1541	P	C <sub>3</sub> A-CaO	45.1	0.0	54.9	42.8	0.0	57.2	
“FeO <sub>1.5</sub> ”-AlO <sub>1.5</sub> system										
(f)	1688	P	Corundum-Spinel	41.2	58.8	0.0	30.9	69.1	0.0	[42]
“FeO <sub>1.5</sub> ”-CaO system										
(g)	1361	P	Hematite-Spinel	0.0	81.7	18.3	0.0	86.4	13.6	[43,44]
(h)	1230	P	CF <sub>2</sub> -Hem	0.0	73.0	27.0	0.0	79.4	20.6	
(i)	1220	P	C <sub>2</sub> F-CF	0.0	71.1	28.9	0.0	77.8	22.2	
(j)	1213	E	CF-CF <sub>2</sub>	0.0	68.7	31.3	0.0	75.8	24.2	
(k)	1440	P	CaO-C <sub>2</sub> F	0.0	46.2	53.8	0.0	55.0	45.0	
“FeO <sub>1.5</sub> ”-CaO-AlO <sub>1.5</sub> system										
Invariant points										
(l)	1324	P	CA-C <sub>2</sub> F-C <sub>3</sub> A	43.3	8.0	48.8	39.6	11.4	49.0	Estimated
(m)	1661	P	Corundum-Spinel-CA <sub>6</sub>	41.6	56.0	2.4	31.5	66.5	2.0	
(n)	1375	P	CA <sub>6</sub> -C(A,F) <sub>3</sub> -CA <sub>2</sub>	24.0	53.0	23.0	18.1	62.8	19.1	Measured
(o)	1260	P	C(A,F) <sub>3</sub> -CA <sub>2</sub> -CA	22.0	48.0	30.0	16.9	57.7	25.4	
(p)	1382	P	C <sub>2</sub> F-C <sub>3</sub> A-CaO	22.0	22.5	55.5	18.6	29.8	51.6	Estimated
(q)	1413	P	Spinel-CA <sub>6</sub> -C(A,F) <sub>3</sub>	20.5	61.0	18.6	15.0	70.0	15.0	Measured
(r)	1210	P	C(A,F) <sub>3</sub> -C <sub>2</sub> F <sub>3</sub> A-CA	19.5	48.8	31.8	14.9	58.4	26.7	
(s)	1205	E	C <sub>2</sub> F <sub>3</sub> A-CA-C <sub>2</sub> F	18.5	49.2	32.4	14.1	58.7	27.2	
(t)	1370	P	Spinel-Hematite-C(A,F) <sub>3</sub>	12.0	68.8	19.2	8.5	76.5	15.0	
(u)	1194	P	C(A,F) <sub>3</sub> -C <sub>2</sub> F <sub>3</sub> A-C <sub>2</sub> F	7.8	59.8	32.4	5.7	68.3	26.0	
(v)	1189	E	C(A,F) <sub>3</sub> -CF-C <sub>2</sub> F	6.3	61.8	31.8	4.6	70.1	25.3	
(w)	1225	P	Hematite-C(A,F) <sub>3</sub> -CF <sub>2</sub>	2.4	69.8	27.8	1.7	76.8	21.5	
(x)	1194	P	C(A,F) <sub>3</sub> -CF <sub>2</sub> -CF	2.0	69.2	28.8	1.4	76.3	22.3	
Saddle points										
(y)	1225	S	C <sub>2</sub> F <sub>3</sub> A-C <sub>2</sub> F	15.0	52.4	32.6	11.3	61.7	27.0	Measured
(z)	1230	S	C <sub>2</sub> F <sub>3</sub> A-C(A,F) <sub>3</sub>	12.5	56.2	31.4	9.3	65.2	25.6	

P, Peritectic; E, Eutectic; S, Saddle point.

phase field has been amended based on findings in the present study.

Figure 5 shows a detail of the liquidus of the “FeO<sub>1.5</sub>”-CaO-AlO<sub>1.5</sub> system in the compositional region of the C(A,F)<sub>3</sub> primary phase field. The liquidus temperature in the C(A,F)<sub>3</sub> primary phase field (marked T) increases with decreasing CaO concentration, from a minimum value of 1189 °C at the point v, corresponding to the C(A,F)<sub>3</sub>-CF-C<sub>2</sub>F eutectic, to a maximum of 1413 °C, at point q, which indicates the equilibrium between the C(A,F)<sub>3</sub>-C(A,F)<sub>6</sub>-spinel phases. The range of temperatures over which the C(A,F)<sub>3</sub> primary phase field is present is in close agreement with Dayal and Glasser<sup>[16]</sup> (1175 °C ~ 1435 °C).

The liquid compositions measured in the present study in the compositional region of the C(A,F)<sub>3</sub> primary phase field are shown in Figure 6. The phase boundaries between C(A,F)<sub>3</sub> and all surrounding phases, hematite, spinel, CA<sub>6</sub>, CA<sub>2</sub>, CA, C<sub>2</sub>F<sub>3</sub>A, CF, and CF<sub>2</sub> have been determined. It can be seen that the low-temperature region extends from point j on the

“FeO<sub>1.5</sub>” – CaO pseudo-binary through points x-v-u-y-s until approximately 20mol pct AlO<sub>1.5</sub>. There are ternary eutectics at point s (liquid-C(A,F)-C<sub>2</sub>(F,A)-C<sub>2</sub>F<sub>3</sub>A) at 1205 °C and point v (liquid-C(F,A)-C(A,F)<sub>3</sub>-C<sub>2</sub>(F,A)) at 1189 °C.

The C<sub>2</sub>F<sub>3</sub>A phase is shown to be an incongruently melting compound with primary phase field bounded by points r-s-y-u-z-r, including the following features:

- (i) the r-z-u boundary between liquid-C(A,F)<sub>3</sub>-C<sub>2</sub>F<sub>3</sub>A;
- (ii) the maximum temperature to which C<sub>2</sub>F<sub>3</sub>A is stable is estimated to be 1230 °C (point z), above which it incongruently melts into liquid and C(A,F)<sub>3</sub>;
- (iii) the s-y-u boundary between liquid-C<sub>2</sub>(F,A) and C<sub>2</sub>F<sub>3</sub>A, with the local maximum at the saddle point y.

The invariant points: the peritectic reactions [liquid-C(A,F)-C<sub>2</sub>(F,A)-C(A,F)<sub>3</sub>] at 1210 °C point r and [liquid-C(A,F)-C<sub>2</sub>(F,A)-C(A,F)<sub>3</sub>] at 1194 °C point u, and the ternary eutectics [liquid-C(A,F)-C<sub>2</sub>(F,A)-C<sub>2</sub>F<sub>3</sub>A]



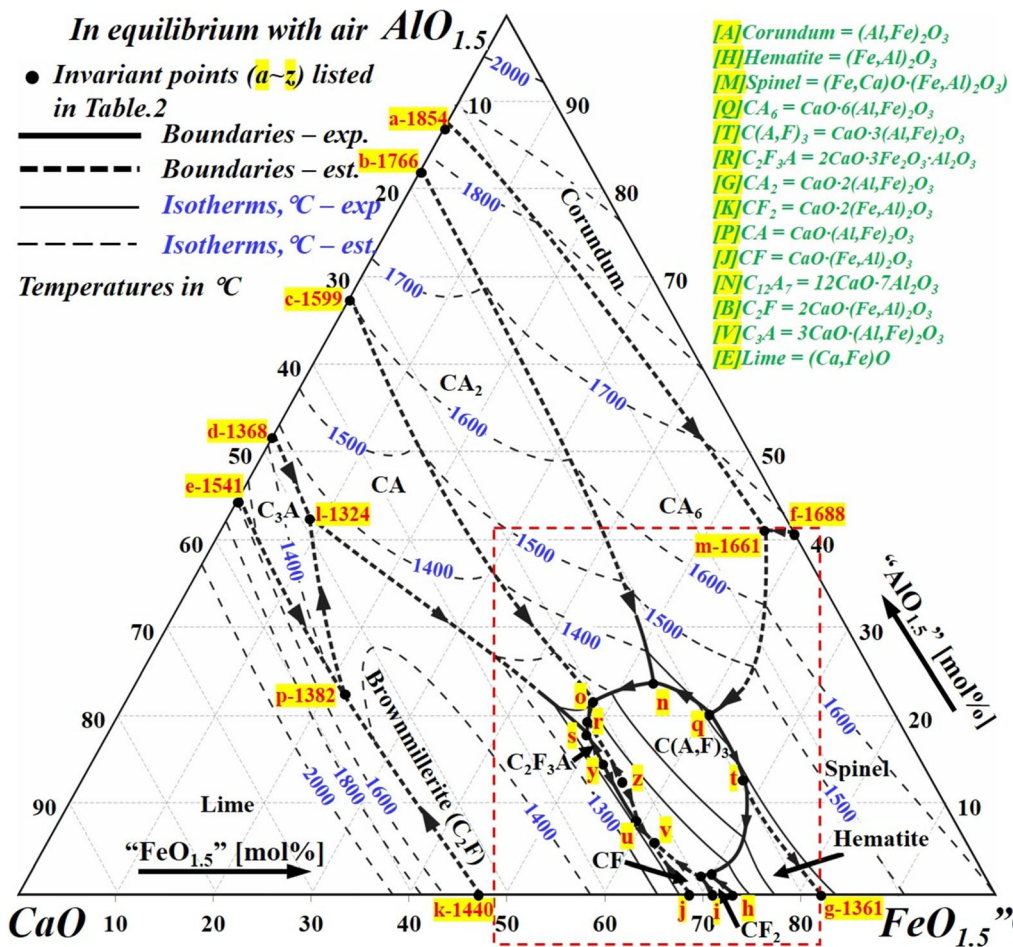


Fig. 4—Proposed liquidus surface of the “ $FeO_{1.5}$ ”- $CaO$ - $AlO_{1.5}$  system in air. Temperatures in °C. Phase boundaries and isotherms greater than 1450 °C are estimated and indicated by dash lines. Details of invariant points (a-z) are listed in Table II.

A] 1205 °C point s in Figure 5 and in Table II, and [liquid-C(F,A)-C (A,F)<sub>3</sub>-C<sub>2</sub>(F,A)] 1189 °C (point v) proposed in the present study differ from the ternary eutectic points [liquid-CA-CF-C<sub>2</sub>F] E3 at 1190 °C, [liquid-CA-CF-C(A,F)<sub>3</sub>] E4 at 1180 °C, and [liquid-C(A,F)<sub>3</sub>-CF-CF<sub>2</sub>] E5 at 1175 °C reported by Dayal and Glasser.<sup>[16]</sup> These differences in findings between the studies are principally due to the presence of the C<sub>2</sub>F<sub>3</sub>A phase. The reason why the absence of C<sub>2</sub>F<sub>3</sub>A in Dayal and Glasser’s study<sup>[16]</sup> may have been due to the difference in experimental techniques. Dayal and Glasser relied principally on the use of optical microscopy and limited X-ray diffraction analysis for phase identification. In contrast, in the present study, significantly more weight has been given to the use of the direct and accurate measurement of phase compositions with EPMA. The C<sub>2</sub>F<sub>3</sub>A is more easily identified under backscattered electron mode rather than under reflected light. The narrow range over which the C<sub>2</sub>F<sub>3</sub>A phase can be formed also helps explain why the presence of this C<sub>2</sub>F<sub>3</sub>A primary phase field was not recognized in earlier investigations.

#### D. Isothermal Sections at Selected Temperatures

The estimated equilibria for the “ $FeO_{1.5}$ ”- $CaO$ - $AlO_{1.5}$  system in air, in the form of isothermal sections at 1200 °C, 1250 °C, 1300 °C, and 1400 °C, are shown in Figures 7(a) through (d). They are estimated with an internal database using FactSage,<sup>[40]</sup> in which the experimental data for the conjugate lines in binary and ternary phase fields obtained in the present study have been incorporated. The extent of solid solutions of the phases at these particular temperatures are taken from the ternary data obtained in the present study (Table I) for the hematite, spinel, C(A,F), C(A,F)<sub>2</sub>, C(A,F)<sub>3</sub>, C(A,F)<sub>6</sub>, and C<sub>2</sub>(F,A), C(F,A), C(F,A)<sub>2</sub>, and C<sub>2</sub>F<sub>3</sub>A phases (plotted on Figures 7(a) through (d)) and the following that were not measured in the current study (corundum, C<sub>2</sub>(F,A) >1300 °C or with high Al<sub>2</sub>O<sub>3</sub>, C<sub>3</sub>(A,F) and CaO), were predicted from the internal database in which previously available experimental data were assessed.<sup>[7,9–13,43,47]</sup> To assist in the readability of the diagram and understanding of the phase relations this complex system, each phase has been designated by capital letters A – V; the legend is provided in

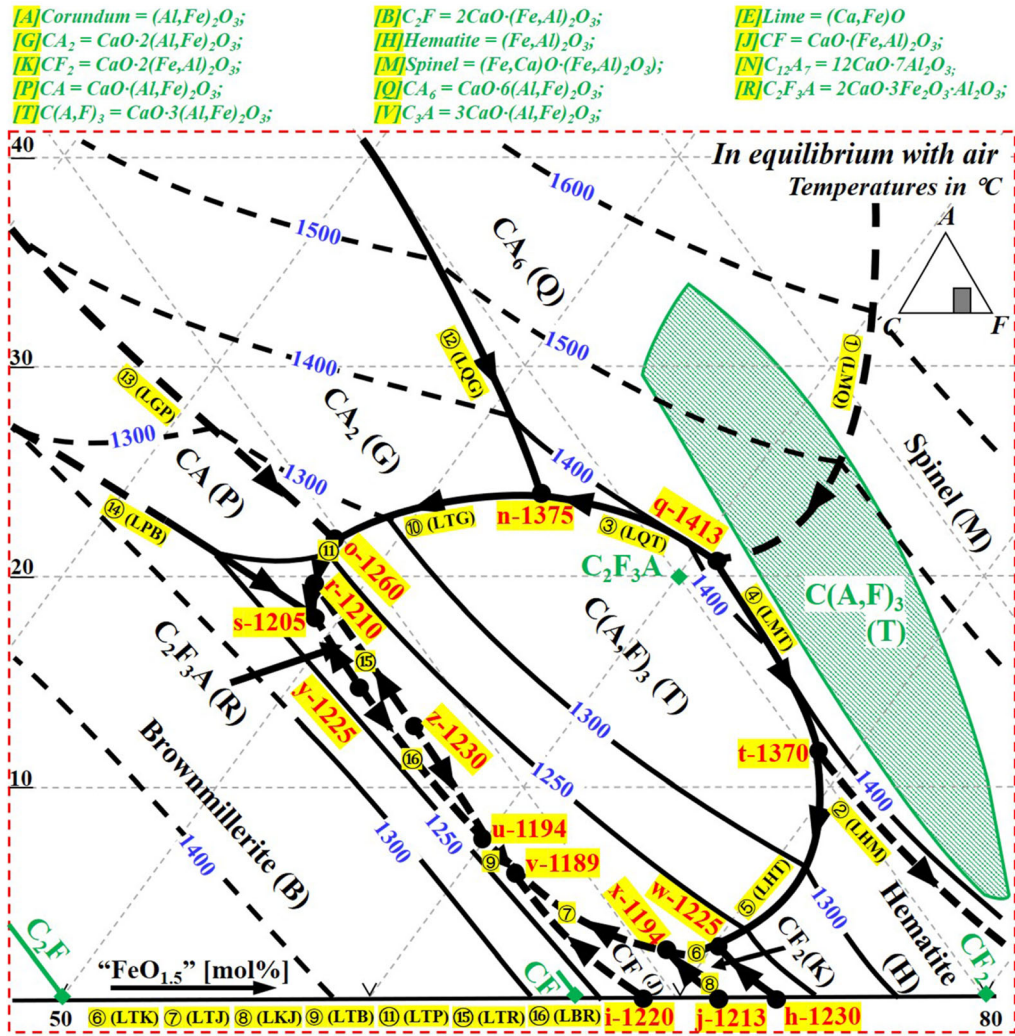


Fig. 5—Detail of liquidus in the “FeO<sub>1.5</sub>”-CaO-AlO<sub>1.5</sub> system in air showing the phase relations of the compositional region of C(A,F)<sub>3</sub> primary phase field. Temperatures in °C. Hatched area is the range of solid solution of T. Details of invariant points (a-z) are listed in Table II. Univariant lines are labeled with numbers and the phases in equilibrium are indicated by the capital letters given in the legend for the ease of presentation.

Figure 7(a). It can be seen that C(A,F)<sub>3</sub> (designated T) is stable over a wide range of compositions at a given temperature with its relative stability decreasing with increasing temperature. Phase relations between the solid-phase C<sub>2</sub>F<sub>3</sub>A and liquid, CA, C<sub>2</sub>F, C(A,F)<sub>3</sub> phases at 1200 °C are presented in Figure 7a.

## V. DISCUSSION

### A. C(A,F)<sub>3</sub> and C<sub>2</sub>F<sub>3</sub>A Solid Compositions

The measured compositions of C(A,F)<sub>3</sub> and C<sub>2</sub>F<sub>3</sub>A solid solutions in equilibrium with the liquid phase at selected temperatures (see Table I) are plotted in Figure 8. The C(A,F)<sub>3</sub> phase identified in the present study is found to have variable C/(A + F) stoichiometry that decreases with increasing temperature rather than lying on the “CA<sub>3</sub>”-“CF<sub>3</sub>” join (constant 14.3 mol pct CaO), as assumed by Dayal and Glasser.<sup>[8]</sup> This observation is in agreement with the findings of Malysheva *et al.*<sup>[18]</sup>

who also reported variable CaO concentrations (12-17 wt pct CaO) in the C(A,F)<sub>3</sub> solid solution from 1130 °C to 1260 °C.

The apparent movement of the towards lower CaO concentration with increasing temperature could be explained by the change in the Fe<sup>2+</sup>/Fe<sup>3+</sup> concentration ratio in the slag with increasing temperature.<sup>[16]</sup> This can result in the partial replacement of Ca<sup>2+</sup> ions in the solid by Fe<sup>2+</sup> ions. It is also possible that some of the iron ions in the lattice sites occupied by Al<sup>3+</sup> and Fe<sup>3+</sup> ions are also replaced by Fe<sup>2+</sup> ions, thus, reducing the Ca<sup>2+</sup> requirement to obtain charge balance.

The AlO<sub>1.5</sub> concentration in the C(A,F)<sub>3</sub> solid solution in equilibrium with liquid is found to be in the range from 3.3 to 33.6 mol pct AlO<sub>1.5</sub> from 1213 °C to 1400 °C, which extends to a lower alumina concentration compared to Dayal and Glasser’s study<sup>[16]</sup> (18.5 ~ 55.5 mol pct CA<sub>3</sub> on the “CA<sub>3</sub>”-“CF<sub>3</sub>” scale, which corresponds to 15.8 ~ 47.6 mol pct AlO<sub>1.5</sub>) on liquidus temperatures at 1140 °C to 1330°C.

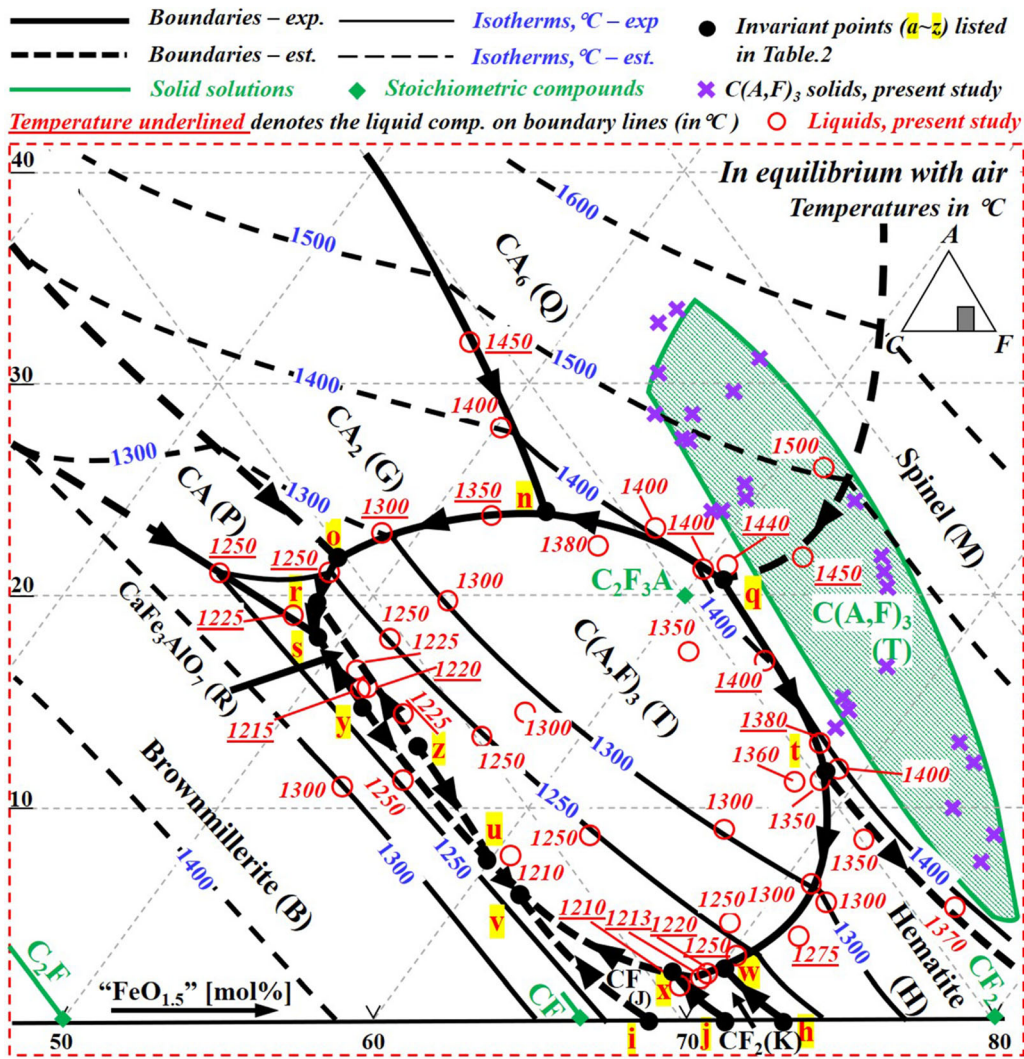


Fig. 6—Detail of the liquidus of the  $C(A,F)_3$  primary phase field in the “ $FeO_{1.5}$ ”- $CaO$ - $AlO_{1.5}$  system in air. Temperatures in  $^{\circ}C$ . The measured liquid compositions and compositions of the corresponding  $C(A,F)_3$  (T) solid solution are also included. Experimental points on the univariant lines are underlined, details of the invariant points (a-z) are listed in Table II.

The  $C_2F_3A$  phase found in the present study is observed to have consistently lower  $CaO$  concentration (~18.6 mol pct) than its stoichiometric composition (20.0 mol pct). This is close to the composition  $Ca_{7.12}Fe_{0.88}^{2+}Fe_{23.82}^{3+}Al_{8.18}O_{56}$  (which corresponds to approximately 17.8 mol pct of  $CaO$ ) reported by Arakcheeva *et al.*<sup>[19,20]</sup> In addition, the  $C_2F_3A$  phase obtained in the present study appears to be a solid solution with the  $Fe^{3+} \leftrightarrow Al^{3+}$  substitution taking place from 18.6 to 21.7 mol pct  $AlO_{1.5}$  from 1150  $^{\circ}C$  to 1225  $^{\circ}C$ .

### B. Extent of $AlO_{1.5}$ in $C(A,F)_3$ Solid Solutions

The  $C(A,F)_3$  compositions listed in Table I are also projected as their  $AlO_{1.5}$  concentrations against equilibrium temperatures (Figure 9). The invariant points, univariant lines, and the solid phases in equilibrium

are also identified by joining these solid compositions as plotted in Figure 9. The  $C(A,F)_3$  solid solution in equilibrium with liquid is found to be stable over the range 3.3–33.6 mol pct  $AlO_{1.5}$  from 1189  $^{\circ}C$  to 1413  $^{\circ}C$ ; this is greater than previously reported by Dayal and Glasser<sup>[8]</sup> but close to that of Malysheva *et al.*

### C. Equilibria Between Liquid and Spinel and Hematite Phases

Details of the equilibria between “ $FeO_{1.5}$ ”- $CaO$ - $AlO_{1.5}$  liquids in air and the hematite (H) and spinel (M) phases obtained in the present study are presented in Figure 10 also included on this diagram are the invariant points associated with the equilibria with the hematite and spinel phases. It is found that alumina is preferentially

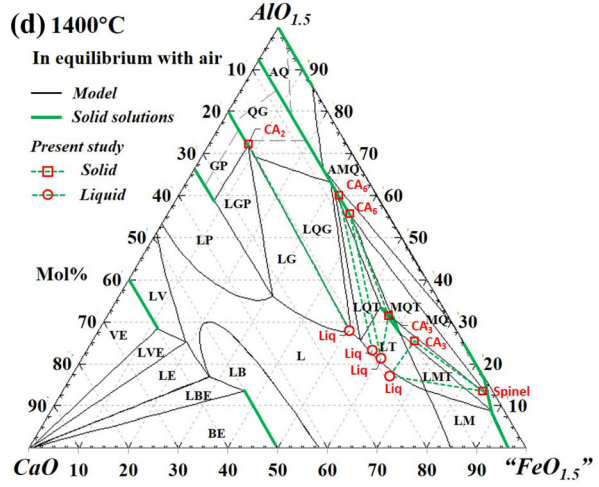
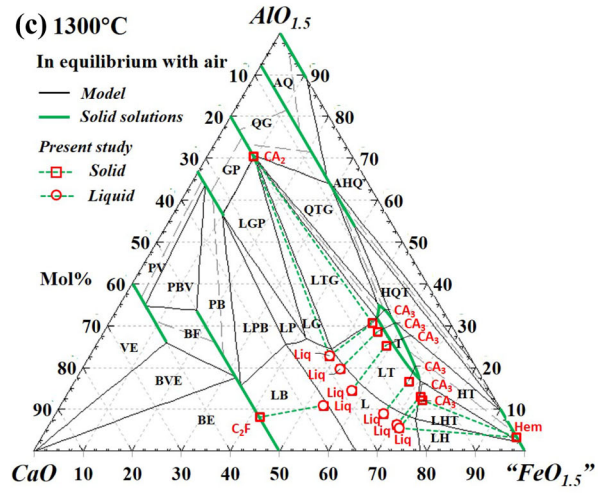
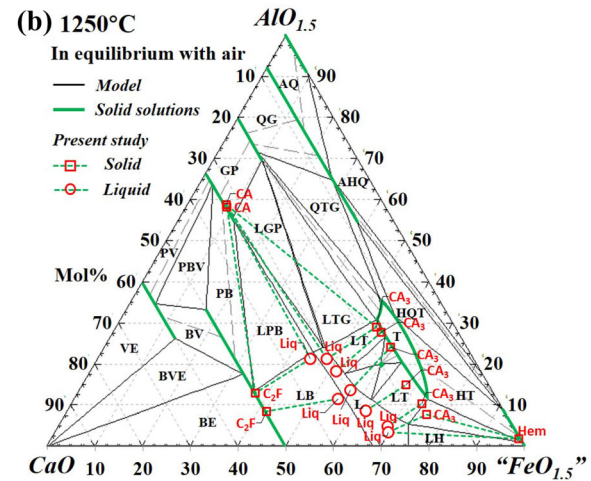
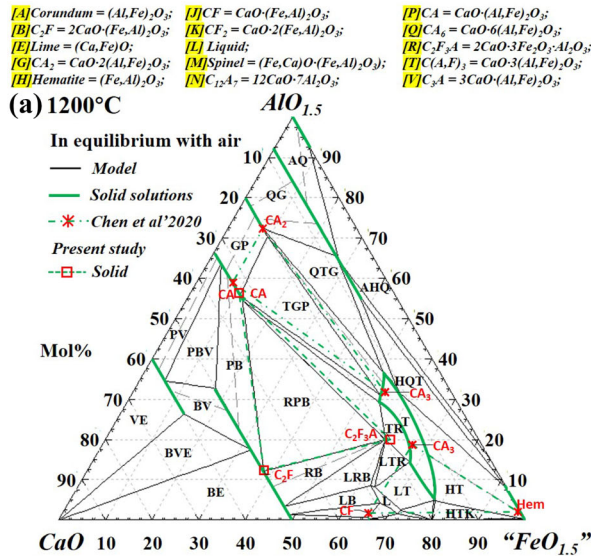


Fig. 7—Experimental data in Table I plotted onto isothermal sections of (a) 1200 °C, (b) 1250 °C, (c) 1300 °C, and (d) 1400 °C, predicted by an internal database using FactSage [40]. Each solid phase is labeled with a designated letter for the ease of presentation.

distributed into the liquid phase over both the hematite and spinel solid phases within the temperature and compositional ranges that have been studied.

In the case of the hematite, the mean distribution ratio of (mol pct Al in the liquid/mol pct Al in the solid) is found to be 1.73 between 1250 °C and 1350 °C; no significant solubility of CaO was found in hematite. For the spinel phase, the mean distribution ratio of (mol pct Al in the liquid/mol pct Al in the solid) is 1.24 between 1370 °C and 1450 °C, and the mol pct CaO in spinel decreases from 3.3 pct at 1370 °C to 1.4 pct at 1450 °C.

The experimental data obtained in the present study have helped to improve the understanding of phase formations during iron ore sintering and will be used for further revision and development of thermodynamic model of the FeO-Fe<sub>2</sub>O<sub>3</sub>-SiO<sub>2</sub>-CaO-Al<sub>2</sub>O<sub>3</sub>-MgO system for iron-making industries.

## VI. SUMMARY

Experimental measurements have been undertaken to determine the liquidus surface of the pseudo-ternary system “Fe<sub>2</sub>O<sub>3</sub>”-CaO-Al<sub>2</sub>O<sub>3</sub> in air with a particular focus on the stability field of C(A,F)<sub>3</sub> (one of the end members of SFCA) in the system. The C(A,F)<sub>3</sub> is an incongruently melting compound having a primary phase field extending from 1189 °C to 1413 °C. The extent of the alumina concentrations in C(A,F)<sub>3</sub> varies with temperature, the minimum is 3.3 mol pct AlO<sub>1.5</sub> at 1213 °C, and the maximum is 33.6 mol pct AlO<sub>1.5</sub> at 1400 °C from the present investigations. The measured solid compositions also indicate a variable CaO concentration in C(A,F)<sub>3</sub> phase extending from below to above stoichiometric CaO concentrations with increasing temperature from 1213 °C to 1400 °C. The extent of the C(A,F)<sub>3</sub> primary phase field is limited by the

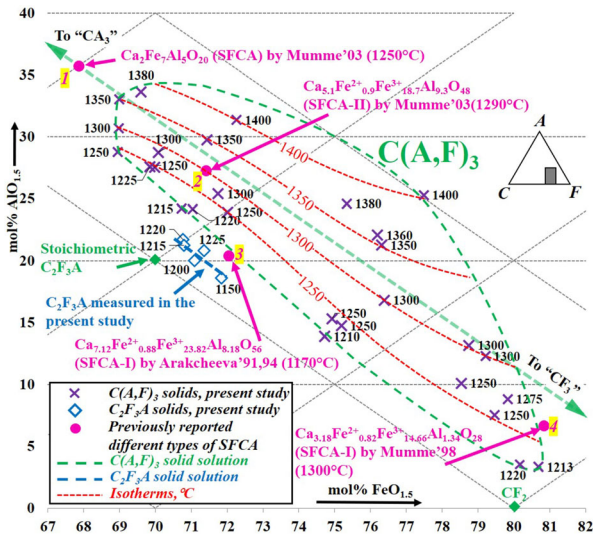


Fig. 8—Isotherms of the C(A,F)<sub>3</sub> solid solution in equilibrium with liquid and compositions of the C<sub>2</sub>F<sub>3</sub>A solid obtained in the present study (compositions of different types of SFCA in this system previously reported by the authors<sup>[19–22]</sup> with their respective preparation temperatures are also plotted as points 1, 2, 3, 4, indicated in Fig. 2).

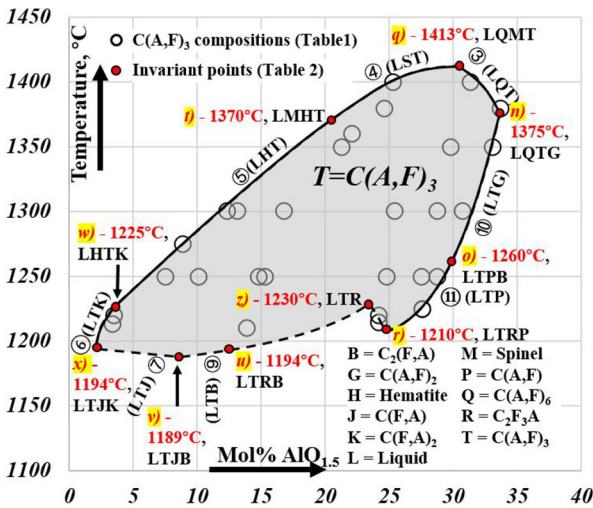


Fig. 9—C(A,F)<sub>3</sub> compositions (mol pct AlO<sub>1.5</sub>) against equilibration temperatures in the “FeO<sub>1.5</sub>”-CaO-AlO<sub>1.5</sub> system in air. Phase boundaries are indicated with numbers as given in Fig. 5, invariant points are indicated with lower-case letters, as listed in Table II.

formation of the following solid phases: CA [CaO·(Al,Fe)<sub>2</sub>O<sub>3</sub>], CA<sub>2</sub> [CaO·2(Al,Fe)<sub>2</sub>O<sub>3</sub>], CA<sub>6</sub> [CaO·6(Al,Fe)<sub>2</sub>O<sub>3</sub>], Hematite [(Fe,Al)<sub>2</sub>O<sub>3</sub>], Spinel [(Fe,Ca)O·(Fe,Al)<sub>2</sub>O<sub>3</sub>], C<sub>2</sub>F [2CaO·(Fe,Al)<sub>2</sub>O<sub>3</sub>], C<sub>2</sub>F<sub>3</sub>A (2CaO·3-Fe<sub>2</sub>O<sub>3</sub>·Al<sub>2</sub>O<sub>3</sub>), CF [CaO·(Fe,Al)<sub>2</sub>O<sub>3</sub>], and CF<sub>2</sub> [CaO·2(Fe,Al)<sub>2</sub>O<sub>3</sub>].

The solid-phase C<sub>2</sub>F<sub>3</sub>A is also found to be an incongruently melting compound, which has been shown to be a solid solution containing between 18.6 and 21.7 mol pct of AlO<sub>1.5</sub> and is stable up to 1225 °C. The C<sub>2</sub>F<sub>3</sub>A solid phase is indicated to be isostructural to SFCA-I according to previous researchers.

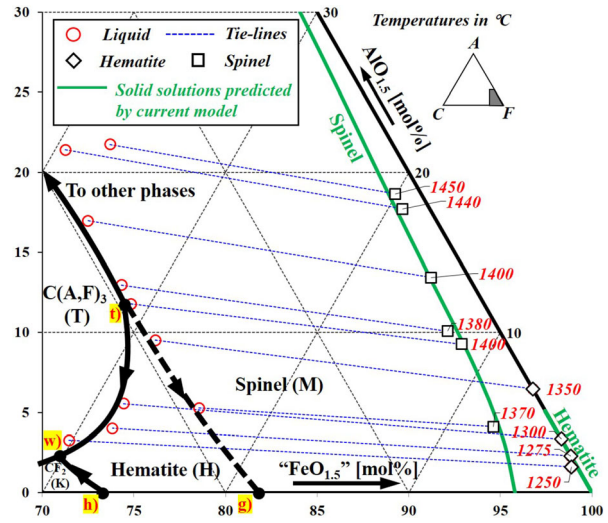


Fig. 10—Tie-lines joining solids (hematite and spinel) and liquids in equilibrium for the system “FeO<sub>1.5</sub>”-CaO-AlO<sub>1.5</sub> in air, invariant points are listed in Table II, temperatures next to solid compositions in °C.

The additional phase equilibria measurements obtained in the present study provide a more complete and more accurate description of the Si-free end member of the SFCA solid solution, an important phase encountered in iron ore-sintering processes.

### ACKNOWLEDGMENTS

The authors would like to acknowledge the Australian Research Council Linkage Program and Altonorte Glencore, Atlantic Copper, Aurubis, Olympic Dam Operation BHP Billiton, Kazzinc Glencore, PASAR Glencore, Outotec Oy (Espoo), Anglo American Platinum, Umicore, and Kennecott Rio Tinto for financial support to enable this research to be carried out, the Centre for Microscopy and Microanalysis, at the University of Queensland for providing electron microscope facilities and the scientific and technical assistance, and Ms. Suping Huang, Ms. Marina Chernishova, and Mr. Shuyi Lou for assistance in experimental work.

### REFERENCES

1. P. Dawson: *Ironmak. Steelmak.*, 1993, vol. 20, pp. 137–43.
2. M.I. Pownceby, J.M.F. Clout and M.J. Fisher-White, *Trans. Instn Min. Metall. Sect.C: Mineral Process Extr. Metall.* 1998, vol. 107, pp. C1-C9.
3. J. Chen, M. Shevchenko, P. Hayes, and E. Jak: *ISIJ Int.*, 2018, vol. 59, pp. 795–804.
4. S. Cheng, M. Shevchenko, Peter C. Hayes and E. Jak, *Metall. Mater. Trans. B* 2019, vol. 51, pp. 1587–1602.
5. J. Chen, M. Shevchenko, P. Hayes, and E. Jak: *ISIJ Int.*, 2019, vol. 59, pp. 805–09.
6. M. I. Pownceby and J. M. F. Clout, *Trans. Inst. Min. Metall., Sect. C* 2000, vol. 109, pp. C36-C48.
7. A. Burdese and C. Brisi: *Annali. Chim.*, 1961, vol. 41, pp. 564–68.

8. J. Chen, S. Cheng, M. Shevchenko, P.C. Hayes, and E. Jak: *Metall. Mater. Trans. B*, 2021, vol. 52b, pp. 517–27.
9. W.C. Hansen, L.T. Brownmiller, and R.H. Bogue: *J. Am. Chem. Soc.*, 1928, vol. 50, pp. 396–406.
10. H.F. McMurdie: *J. Res. NBS*, 1937, vol. 18, pp. 475–84.
11. C. Brisi, *Annali Chim.* 1954, vol. 44, p. 510.
12. T.F. Newkirk and R.D. Thwaite: *J. Res. Nat. Bur. Stand.*, 1958, vol. 61, pp. 233–45.
13. C.M. Schlaudt and D.M. Roy: *Nature (London)*, 1965, vol. 206, p. 819.
14. T.R.C. Patrick and M.I. Pownceby: *Metall. Mater. Trans. B*, 2002, vol. 33B, pp. 79–89.
15. M. Allibert, H. Gaye, J. Geiseler, D. Janke, B. J. Keene, D. Kirner, M. Kowalski, J. Lehmann, K. C. Mills, D. Neuschutz, R. Parra, C. Saint-Jours, P. J. Spencer, M. Susa, M. Tmar and E. Woermann: *Slag Atlas*, 1995, p. 127.
16. R. R. Dayal and F. P. Glasser, *Sci. Ceram.* 1967, vol. 3, pp. 199, 203, 205–207.
17. D.H. Lister and F.P. Glasser: *Trans. Br. Ceram. Soc.*, 1967, vol. 66, pp. 293–305.
18. T. Y. Malysheva, I. V. Ostrovskaya, V. Y. Lyadova, M. S. Model and V. I. Ponomarev, *Izv. Akad. Nauk SSSR, Met.* 1976, vol. No 5, pp. 78–86.
19. A.V. Arakcheeva, O.G. Karpinskii, and V.Ya. Lyadova: *Kristallografiya*, 1991, vol. 36, pp. 603–11.
20. A.V. Arakcheeva and Zh. Strukt.: *Khim. (Zhurnal Strukturnoi Khimii)*, 1994, vol. 35, pp. 85–96.
21. W. G. Mumme, *Neues Jahrb. Mineral., Abh.* 2003, vol. 178, pp. 307–335.
22. W. G. Mumme, J. M. F. Clout and R. W. Gable, *Neues Jahrb. Mineral., Abh.* 1998, vol. 173, pp. 93–117.
23. W. G. Mumme, *Neues Jahrb. Mineral., Monatsh.* 1988, pp. 359–66.
24. J. D. G. Hamilton, B. F. Hoskins, W. G. Mumme, W. E. Borbidge and M. A. Montague, *Neues Jahrb. Mineral., Abh. (Neues Jahrbuch fuer Mineralogie, Abhandlungen)* 1989, vol. 161, pp. 1–26.
25. S. Nicol, J. Chen, M. I. Pownceby and Nathan A. S. Webster, *ISIJ int.* 2018, vol. 58, pp. 2157–72.
26. E. Jak, P. C. Hayes and H. G. Lee, *Met. Mater. (Seoul, Repub. Korea)* 1995, vol. 1, pp. 1–8.
27. E. Jak, In *9th Intl. Conf. on Molten Slags, Fluxes and Salts (MOLTEN12)*, The Chinese Society for Metals: Beijing, China, 2012, p. W077.
28. J. Chen, M. Shevchenko, P.C. Hayes, and E. Jak: *ISIJ Int.*, 2019, vol. 59, pp. 795–804.
29. M. Shevchenko and E. Jak: *Metall. Mater. Trans. B*, 2019, vol. 50B, pp. 2780–93.
30. M. Shevchenko and E. Jak: *Ceram. Int.*, 2019, vol. 45, pp. 6795–6803.
31. J. Philibert, *X-Ray Opt. X-Ray Microanal., 3rd Intl. Symp., Stanford Univ.* 1963, pp. 379–92.
32. P. Duncumb and S.J.B. Reed: *Quantitative Electron Probe Microanalysis*, 6th ed., K.F.J. Heinrich, ed., NBS Spec. Publ. 298, US Dept. Commerce, 1968, pp. 133–54.
33. P. Duncumb, *Electron Microsc. Anal., Proc. Anniv. Meet., 25th* 1971, pp. 132–37.
34. S. Nikolic, P.C. Hayes, and E. Jak: *Metall. Mater. Trans. B*, 2009, vol. 40B, pp. 892–99.
35. A. Fallah-Mehrjardi, T. Hidayat, P.C. Hayes, and E. Jak: *Metall. Mater. Trans. B*, 2017, vol. 48B, pp. 3002–16.
36. M. Shevchenko and E. Jak: *J. Phase Equilib. Diff.*, 2019, vol. 40, pp. 319–55.
37. M. Timucin and A.E. Morris: *Metall. Trans.*, 1970, vol. 1, pp. 3193–3201.
38. E. Jak, P. Hayes, A. D. Pelton and S. A. Decterov, In *Proc. VIII Int'l Conf. on Molten Slags, Fluxes and Salts*, (Santiago, Chile, 2009), pp 473–90.
39. S. A. Decterov, I.-H. Jung, E. Jak, Y.-B. Kang, P. Hayes and A. D. Pelton, In *SAIMM Symposium Series S36 (VII Int. Conf. on Molten Slags, Fluxes & Salts)*, ed. C. Pistorius (The South African Institute of Mining and Metallurgy, Johannesburg, Republic of South Africa: 2004), pp 839–50.
40. *FactSage*. (Ecole Polytechnique, Montréal, <http://www.factsage.com/>, 2008).
41. G. Eriksson and A.D. Pelton: *Metall. Trans.*, 1993, vol. 24, pp. 807–16.
42. V. Prostavkova, D. Shishin, M. Shevchenko, and E. Jak: *CAL-PHAD*, 2019, vol. 67, p. 101680.
43. T. Hidayat, D. Shishin, S.A. Decterov, and E. Jak: *Metall. Trans. B*, 2016, vol. 47B, pp. 256–81.
44. S. Cheng, M. Shevchenko, P.C. Hayes, and E. Jak: *Experimental Phase Equilibria Studies in the FeO-Fe<sub>2</sub>O<sub>3</sub>-CaO system*, private communication, The University of Queensland, Brisbane, QLD, PYROSEARCH, 2020.
45. R.W. Nurse, J.H. Welch, and A.J. Majumdar: *Trans. Brit. Ceram. Soc.*, 1965, vol. 64, pp. 409–18.
46. R.W. Nurse, J.H. Welch, and A.J. Majumdar: *Trans. Brit. Ceram. Soc.*, 1965, vol. 64, pp. 323–32.
47. D. Shishin, V. Prostavkova, E. Jak, and S. Decterov: *Metall. Mater. Trans. B*, 2016, vol. 47B, pp. 397–424.

**Publisher's Note** Springer Nature remains neutral with regard to jurisdictional claims in published maps and institutional affiliations.